Bachelor Thesis

Degree project in computer science and engineering 15HP

Position estimation for indoor navigation

Halmstad 2024/03/22
Shahidullah Hassanzadah & Heri Ndami

HALMSTAD UNIVERSITY

Acknowledgment

We extend our heartfelt gratitude to our families and friends for their unwavering support throughout this project. A special acknowledgment goes to our esteemed supervisors, Elena Haller and Oscar Molina, whose invaluable guidance and encouragement propelled us forward. Additionally, we wish to thank Thomas Lithén for generously providing the essential hardware to realize our goals.

Abstract

This project investigates developing and implementing innovative indoor navigation systems by leveraging repurposed Wi-Fi infrastructure and dedicated RFM69HCW transceivers. Aimed at enhancing indoor positioning accuracy, the study explores the viability of using Received Signal Strength Indicator (RSSI) and dedicated device localization techniques to overcome the limitations of existing Global Positioning System (GPS) technology in indoor environments. Through the design and testing of a printed circuit board (PCB) prototype that connects Raspberry Pi Pico (RPP) to RFM69HCW modules and the development of custom drivers for the RP2040 processor, this research addresses the challenges of indoor navigation, such as signal variability and environmental interference. The project also emphasizes the importance of sustainable technology development by repurposing electronic waste for innovative applications. Findings from the study reveal the potential of these methodologies to improve indoor positioning accuracy despite challenges related to hardware compatibility and the dynamic nature of indoor spaces. This research contributes to indoor navigation by demonstrating the feasibility of using repurposed and dedicated hardware solutions, offering insights into future directions for enhancing indoor navigation systems, and highlighting the role of sustainability in technological innovation.

Sammanfattning

Detta projekt utforskar utvecklingen och implementeringen av innovativa system för inomhusnavigering genom att återanvända befintlig Wi-Fi-infrastruktur samt dedikerade RFM69HCW-sändtagare. Med målet att förbättra noggrannheten i inomhuspositionering undersöker studien möjligheten att använda tekniker för mottagen signalstyrkeindikator (RSSI) och dedikerad enhetslokalisering för att övervinna begränsningarna med befintlig GPS-teknologi i inomhusmiljöer. Genom design och testning av en prototyp för kretskort (PCB) som ansluter Raspberry Pi Pico (RPP) till RFM69HCW-moduler, samt utveckling av anpassade drivrutiner för RP2040-processorn, adresserar denna studie, utmaningarna med inomhusnavigering såsom signalvariabilitet och miljömässig interferens. Projektet betonar även vikten av hållbar teknikutveckling genom att återanvända gamla enheter för innovativa tillämpningar. Studiens resultat visar på potentialen hos dessa metoder att förbättra noggrannheten i inomhuspositionering, trots utmaningar relaterade till hårdvarukompatibilitet och den dynamiska naturen hos inomhusutrymmen. Denna studie bidrar till fältet för inomhusnavigering genom att demonstrera genomförbarheten av att använda dedikerad hårdvarulösningar, erbjuder insikter i framtida arbete och förbättring av system för inomhusnavigering som lyfter fram rollen av hållbarhet i teknologisk innovation.

Table of contents

1. Introduction

Navigation has been an essential aspect of our lives, and humans have continually been developing new and better tools for navigation, from celestial navigation using the stars to the invention of compasses and the art of interpreting hand-drawn maps. These endeavors eventually culminated in the developing the Global Positioning System (GPS), which has transformed outdoor navigation for countless individuals worldwide.

Nevertheless, despite these remarkable advancements in navigation technology, intricate and challenging terrains remain closer to us than we might initially perceive. Although often overlooked, indoor navigation can be essential, especially in today's modern society, where large-scale constructed buildings have become commonplace, and effective indoor navigation must be addressed.

In our observation of visiting multiple malls and other large buildings, we have observed that wayfinding is facilitated through various means. Many malls employ paper maps or electronic displays strategically placed throughout the premises to assist visitors in navigating the complex layout of the building. These visual aids provide crucial information about the location of stores, facilities, and other points of interest.

Taking a closer look at our academic institution, Halmstad University, we find an innovative approach to indoor navigation by utilizing a mobile application called MazeMap. This application, designed to assist users in navigating around the campus, visually showcases the layout of the building and the selected floor. However, it's important to note that MazeMap does not provide precise indoor location information for the users. This limitation stems from GPS technology's constraints when attempting to offer accurate positioning for indoor users. Consequently, individuals unfamiliar with the campus may need help navigating effectively.

Considering these challenges, a pressing need arises for developing a more refined and accurate indoor positioning system. One that can detect which room a user is in. Addressing this gap in technology could revolutionize how individuals navigate within indoor spaces, ensuring a smoother and more user-friendly experience for all.

This project, envisioned by the authors, aims to tackle the challenge of electronic waste (e-waste) by focusing on repurposing and offering innovative ways to utilize old hardware. The project is done independently without a specific external project provider.

1.1 Project goals

This project aims to explore two methods for enhancing indoor position accuracy and determine if these methods are worth implementing. The first method is leveraging repurposed old Wi-Fi infrastructure as a network of location anchors for device tracking. The investigation will focus on the advantages of the **R**eceived **S**ignal **S**trength **I**ndicator (RSSI) and potential signal processing techniques to estimate a device's location within the Wi-Fi signal's coverage.

The goal is to achieve a high level of accuracy in determining device locations, with a target precision of one meter. This level of precision is justified by recognizing that a one square meter area is typically the space occupied by a single person. Therefore, achieving this level of accuracy ensures pinpointing the location of individual devices with the same detail as human occupancy, enabling various applications such as asset tracking, navigation, and proximity-based services.

Another method to be explored involves utilizing a dedicated embedded system for device localization, explicitly employing the RFM69HCW transceiver operating in the license-free 435 MHz band[1], which aligns with the objectives of this project. The RFM69HCW does not come with a pre-installed antenna, giving users the flexibility to deploy antennas that meet their specific requirements, in our case, an antenna that provides an omnidirectional radiation pattern. This approach also incorporates RSSI techniques for location estimation.

However, the limitation of the RFM69HCW necessitates pairing it with the **R**aspberry **P**i **P**ico (RPP) for data processing. This introduces a combability challenge, as the existing drivers designed for the ATMega chipset are incompatible with the RP2040 processor and the C/C++ language utilized in the RPP Software Development Kit (SDK), thus requiring the development of new drivers.

The project's objective is to assess the accuracy of the investigated methods in determining whether a device is located within a specific room. This introduces precision constraints that must be met to fulfill the requirement accurately.

The goals we aim to reach with this project are as follows:

- Investigating whether 802.11 network-based (i.e., Wi-Fi) hardware can be repurposed and utilized as tracking hardware.

- Developing drivers for the RP2040 C/C++-SDK to work with the RFM69HCW transceiver.
- Designing a **p**rinted **c**ircuit **b**oard (PCB) prototype for connecting the RPP and the RFM69HCW hardware with additional components for easy debugging.
- Achieving position precision accuracy below 100 cm.

The purpose of this project.

- Reduce e-waste by giving existing Wi-Fi infrastructure a new purpose, which extends their lifecycle, maximizes their utility, and provides more ways of working with current hardware, which has a positive environmental aspect.

2. Background

This section will present the concept and development of an indoor navigation system, particularly for large buildings. An overview of the technology's development, essential components, and architectural frameworks will all be included. Additionally, we will focus on integrating user interfaces and data processing infrastructures, highlighting critical innovations, and finding obstacles in the area. This overview provides a basic understanding of our approach to developing an advanced indoor navigation system that addresses the special navigation needs found within extensive, complex facilities.

2.1 Global Positioning System (GPS)

When we venture into unfamiliar outdoor territories, we rely on tools like GPS to streamline the process of determining our location and charting the path to our desired destination. GPS operates by utilizing an array of satellites orbiting the Earth with remarkable precision. These satellites house atomic clocks that maintain extreme accuracy, continuously transmitting their location and time data to receivers on the ground. These receivers employ trilateration and various sophisticated algorithms to calculate the receiver's precise location[2].

For simplicity reasons, imagine a receiver in a two-dimensional coordinate system that represents a surface on earth, and the location of this device is unknown; however, this receiver can communicate with other devices that know their location; let us call these devices satellites, denoted (S1, S2, S3) and the receiver A as illustrated in Figure 1.

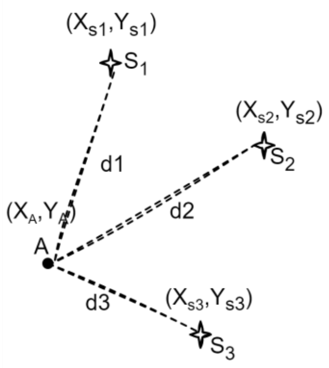

Figure 1: A presentation of receiver A in an unknown position with the satellite in their known position

By synchronizing the clocks of every device in this system, a signal can be sent from every satellite to the receiver, thus retrieving the information of when the signal was sent and received. The time stamp data can be utilized to calculate the time it took for the signal to propagate through space to reach the receiver $\Delta t = t_{send} - t_{received}$. Using the distance formula that states distance = speed x time and the speed of radio waves (light) denoted c in free space, we can calculate the distance between the receiver and the satellite as d = c x Δt. Since the position of the satellites are known and the respective distances are calculated, a linear equation can be set using the Pythagoras theorem to solve for the position of the unknown receiver, see Equation 1.

$$\begin{cases}(x_a - x_{s1})^2 + (y_a - y_{s1})^2 = {d_1}^2 \\ (x_a - x_{s2})^2 + (y_a - y_{s2})^2 = {d_2}^2 \\ (x_a - x_{s3})^2 + (y_a - y_{s3})^2 = {d_3}^2\end{cases}$$

Equation 1: For pinpointing user location (a) using distance measurement from fixed reference points S_i.

Each equation represents a circle at position (x_s, y_s) with radius d. The point (x_a, y_a) that satisfies the equation system is the point where all three circles intercept which translates to where the unknown receiver is; see the illustration in Figure 2. However, distance calculations often contain errors in real-world scenarios, which can be mitigated by employing linear regression to determine the optimal position.

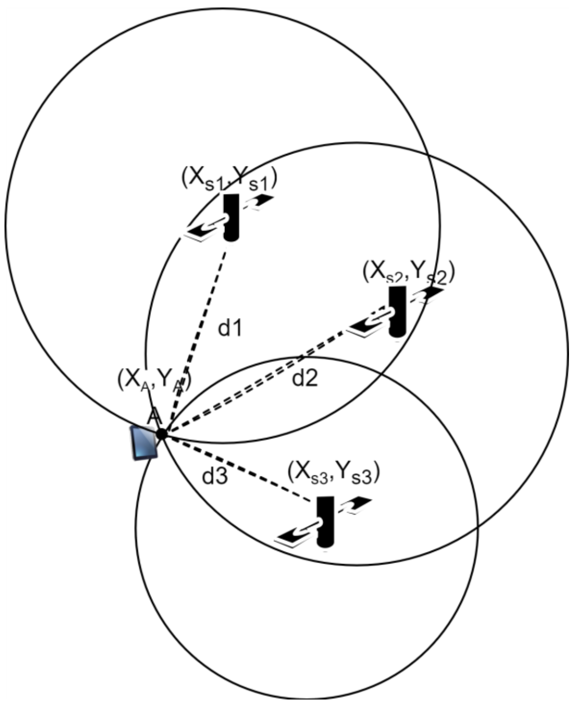

Figure 2: intersection point of all distances.

The simplified explanation of GPS operation, while helpful for understanding the basics, doesn't capture the complete picture. However, it provides insight into trilateration calculation, the basis for implementing indoor location finding. Real-world factors like kinetic and gravitational time dilation introduce errors in the synchronized clocks. These errors arise from the satellites' high speed (causing kinetic time dilation) and their higher altitude (experiencing less gravitational time dilation than us on the ground). Additionally, most receivers need more extreme precision of the satellite clocks, further hindering perfect synchronization.

To overcome these challenges, the system continuously updates the receiver's clock using information sent from the satellites. This constant adjustment ensures the accuracy of the positioning data, making GPS the reliable tool we know today.

However, regarding indoor navigation, GPS must meet the required accuracy standards. The challenge lies in the intricate and confined nature of indoor spaces, which hinder the reception of signals from satellites by bouncing off walls and impede the system's ability to pinpoint locations with the same degree of accuracy as outdoors.

2.2 Other Works

This section reviews existing research and projects related to our field, highlighting key contributions and advancements. This examination allows us to acknowledge prior achievements while identifying gaps and opportunities for our project. By critically assessing these works, we position our research within the broader context, showcasing how our project builds upon, complements, or diverges from previous efforts. This section emphasizes the novelty of our work and its potential impact, providing a foundation investigation and underscoring its significance in advancing the field.

2.2.1 Combined AoA and RSSI

J. R. Jiang et al (2013) developed a wireless sensor network (WSN) positioning method that was created using a combination of signal strength (RSSI) and angle of arrival (AoA) analysis and utilization techniques. AoA Localization with RSSI Differences (ALRD) is the name of this method. This method uses innovative approaches to improve positioning accuracy by using quadratic and linear regression analysis in the context of specially aligned antennas. During the preparatory phase of the process, the RSSI values will conform to a parabolic AoA function, which is 0–90°[3].

This is achieved using quadratic regression analysis, a statistical method that creates a parabolic relationship that shows the relationship between RSSI values and AoA. This investigation must be done to predict RSSI values from different viewing angles to achieve high localization accuracy. It uses two antennas directed toward each other and placed in the same place to improve localization accuracy. Measuring the differences in RSSI values between these antennas refines the information required for an even more accurate position determination. Then, linear regression analysis is used to correct these differences into a linear AoA function. The ALRD location scheme is presented with these plans. Using quadratic and linear regression analysis functions, it can locate a sensor node's position. In this way, two quad nodes are used, each with two aimed antennas perpendicular to each other, allowing them to be precisely located within a specific area. Using this method in an indoor environment with a survey area showed that the average localization error was 124 centimeters per square meter (m^2) when two quad nodes were mounted at opposite corners [3].

To reduce this error, two advances were made: maximum point minimum diameter and maximum point minimum rectangle. These techniques aim to collect many four-node signals within one second to discover the most densely populated set of estimated positions. They reduced the typical localization error by about 29% to 89 cm. This method demonstrates how sophisticated statistical analysis and innovative antenna orientation can improve wireless sensor network localization accuracy; this opens new possibilities for precise indoor positioning [3].

2.2.2 Position Finding with pre-calculated Signal Path.

J. Dong et al (2019) developed the technology for indoor navigation based on smartphones to address the significant demand for interior navigation services. Unfortunately, their acceptance has been comparatively slow since there aren't many accurate and detailed indoor maps available; this may be because infrastructure-based indoor localization solutions may be expensive to build and maintain. A scalable and economical indoor mapping, localization, and navigation system based on smartphone-derived inertial and visual sensor data. ViNav finds points of interest in 3D models, creates navigation meshes for pathfinding, and uses structure-from-motion approaches to reconstruct 3D models of indoor spaces from crowdsourced pictures. ViNav uses image-based localization, which determines the positions and facing directions of users, and uses this capability to calibrate user trajectories based on dead reckoning and sensor fingerprints gathered along the trajectories. Building more detailed and targeted interior maps and reducing the time for localization requests to respond are two uses for the alienated data. ViNav's innovative use of sensor and optical data and crowdsourcing techniques allows it to provide smartphone users with cost-effective and precise indoor navigation services [4].

2.2.3 UWB Techniques

T. H. Riehle et al (2008) developed the Ultra-Wideband (UWB) technology for indoor navigation to provide precise real-time location tracking for visually impaired individuals. The module can send location data to the user`s handheld computer using a commercial asset monitoring system and provide accurate position measurements. This system reforms the user's power to navigate indoor environments by using the user's current location and desired destination to generate personalized routing messages. The navigation system's architecture incorporates ideas from research on language-based spatial learning. This system aims to innovate navigation direction perception and reduce the cognitive load on the user by using accurate distance measurements in speed and relative and absolute direction information. Human trials have shown the technology to work better than conventional methods, such as using a guide dog or a long cane, suggesting it has the potential to improve independence and accessibility for the visually impaired indoors significantly [5].

2.2.4 Estimation with Beamforming

Beamforming is a signal processing technique that focuses the signals in a specific direction by adjusting the phase and amplitude of multiple antennas, enhancing signal quality, and reducing interference[6]. This technique can be utilized for position estimation by focusing the beam to different angles at different instances, see Figure 3. The angle information can be encoded in the carrier wave, which is then processed at the receiver end and combined with the signal strength information to estimate the receiver's location, thus substantially reducing the number of AP nodes required. When determining the coordinates (X, Y) based on the known values d, θ, and (X_{AP}, Y_{AP}), trigonometric relationships come into play. Specifically, X is calculated by adding the displacement in the x-direction (d * cos(θ)) to the initial x-coordinate (X_{AP}). At the same time, Y is determined by adding the displacement in the y-direction (d * sin(θ)) to the initial y-coordinate (Y_{AP}). However, since the desired working environment is indoors, the signal will bounce on objects and walls must be considered. One approach to resolving this issue involves simulating potential bouncing paths within the environment where the measurements are conducted. This simulation generates data reflecting the expected signal strength at various beamforming angles. If the received signal strength falls below the expected value, it suggests the presence of multipath interference, allowing the signal to be neglected.

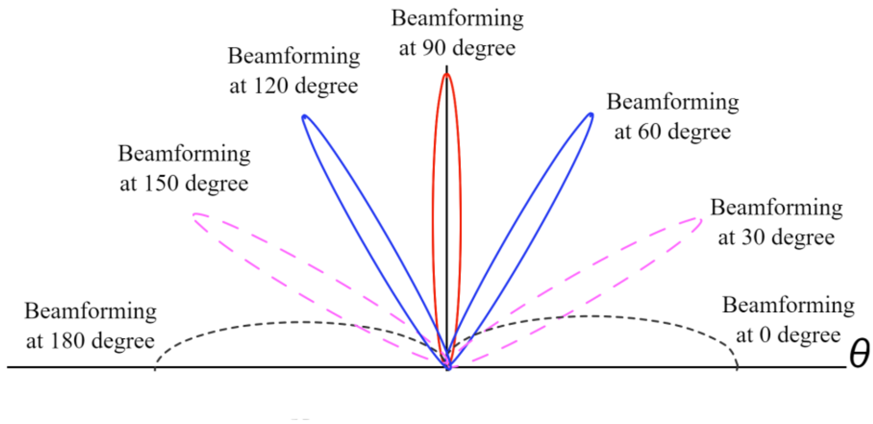

Figure 3. A description of possible angles that can be done with beamforming.

Figure 4 shows the transmission of a signal from an access point employing beamforming technology, which directs the signal at a precise angle to enhance communication with the receiving device.

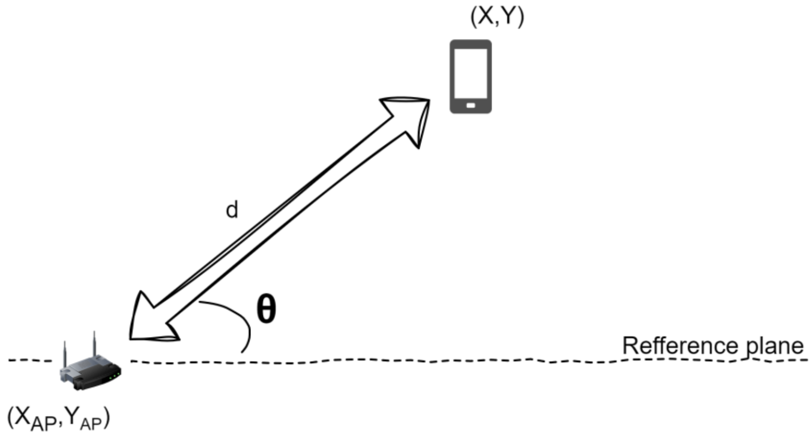

Figure 4. A signal is transmitted from an AP to a receiver at an angle.

2.2.5 Position Estimation with Angle of Arrival (AoA)

The idea here is quite like the beamforming method however, instead of sending the signal at a specific angle, the signal is received at the angle of arrival, which is measured using multiple antennas and then combined with the RSSI information, which provides a distance estimation to calculate the estimated location[7], [8].

2.2.6 The Multiple Signal Classification (MUSIC)

To address this issue, a practical solution involves employing an array of antennas to estimate the angle of arrival precisely. In the work presented in [8], an array of antennas was harnessed to gather the angle of arrival data. This was achieved by representing the phase shift between the signals received by M antennas as a complex exponential, as depicted in Equation 2.

Subsequently, the multiple signal classification (MUSIC) algorithm was applied, utilizing an eigenspace method to estimate the angle of arrival accurately.

$$\Phi(\theta) = e^{-\frac{j2\pi \sin(d)}{\lambda}}$$

$$\overrightarrow{a(\theta)} = [1 \;\; \Phi(\theta) \;\; \Phi(\theta)^2 \;\; \dots \;\; \Phi(\theta)^{M-1}]$$

Equation 2. An expression of the phase shift (Φ) vector on antennas to determine the M-1 angle of arrival and $\overrightarrow{a(\theta)}$ denotes a vector related to the spatial signature profile of a received signal at an angle θ.

Using an eigenspace method, the multiple signal classification (MUSIC) algorithm addresses multipath challenges by estimating the Angle of Arrival (AoA) for numerous signals. It forms steering vectors for each signal source by representing the phase shift between M antennas as complex exponentials.

If you have an array with M antennas and a signal with a correlation matrix Rxx, it's proven that some special vectors in Rxx are perpendicular to the steering vectors. This concept is used in calculating the MUSIC spectrum, see Equation 3.

$$P_{MU}(\theta) = \frac{1}{\vec{a}(\theta)^H E_N E_N^H \vec{a}(\theta)}$$

Equation 3. The function is to find the music spectrum; P is power, representing signal likelihood, and E is a matrix for compensating noise.

MUSIC requires more antennas than paths to resolve accurately. In practice, it can differentiate up to M - 1 paths, so with three antennas, only two multipath signals can be distinguished. FPGA-based radios are used to overcome this, combining two 3-antenna NICs into a 5-antenna array. Spatial smoothing leverages the relationship between measurements across antennas and frequencies, especially in Wi-Fi, forming a virtual measurement using frequency diversity and signal time of flight.

Another technique to solve the position estimation was utilizing the multidimensional scaling map (MDS-MAP) [9]. This is done by placing multiple pairs of sensors around an area and having only some of the sensor positions known. An algorithm that estimates the distance to the nearest sensor using information from signal strength and the probability of the other sensor's location is used to estimate the receiver's location.

This method's computational demands are substantial, which poses a significant obstacle to its practical implementation in navigation. As a result, it would substantially increase calculation time, causing the system to perform at an exceptionally slow pace.

2.3 State Of the Art

Our project's current state illustrates two main strategies for creating an indoor position estimation. First off, we're recycling outdated hardware in an inventive way and making use of available resources to develop a workable solution. We can minimize costs and maximize usefulness with this approach.

Second, we're exploring embedded systems and explicitly utilizing the RFM69HCW module in conjunction with the Raspberry Pi Pico. This combination might provide improved accuracy and dependability in indoor positioning. However, these need to be provided with the correct drivers, which forces us to develop those drivers that facilitate communication between RPP and RFM69HCW.

Our goal is to create a state-of-the-art indoor position finder that balances precision, dependability, and affordability by combining these approaches. Our goal is to develop a flexible tool capable of pinpointing a user's location within a specific room within a large building.

2.4 Theoretical Framework

In this section, we present the theoretical framework that underpins the execution of the project, focusing on the key technological components and concepts that are the foundation for the project’s design and implementation. Through a detailed examination of each technical aspect, we aim to understand better how these technologies interact to fulfill the project's objectives.

2.4.1 Free Space Propagation

In an ideal condition, Equation 4, Friis transmission equation describes the received power by an antenna system from a transmitting antenna through free space. This provides a comprehensive framework for understanding the relationship between transmitted power, antenna gains, distance, wavelength, and path loss in wireless communication systems. As described in Equation 5, the path loss is also derived from Equation 4; however, it is converted in decibels (dB) to offer significant practical advantages in simplifying analysis, facilitating comparison, and standardization.

RSSI is typically measured in dBm, representing signal strength. In ideal conditions, such as free space, RSSI can be used to estimate distance using the Friis formula. However, real-world environments introduce factors that impact signal propagation, rendering direct distance calculation impractical. Despite this, the fundamental characteristics of the system remain consistent.

The relationship between distance and RSSI follows the path loss formula characteristic, even though it deviates from the ideal scenario. The equation typically involves deriving distance from RSSI in positioning systems where distance calculation is crucial. This is the inverse of the path loss formula, resulting in an exponential relationship. Hence, the characteristic of this function resembles that of the inverse function of the path loss formula, exhibiting an exponential behavior.

$$P_r = \frac{P_t * G_t * G_r * \lambda^2}{(4\pi d)^2}$$

Equation 4: Friis transmission equation, Pr = received power, Pt = transmitted power, Gr received gain, Gt transmitter gain, and d is the distance between the antennas.

$$FSPL(dBm) = 20log_{10}(d) + 20log_{10}(f) + 20log_{10}(\frac{4\pi}{c})$$

Equation 5: The free space path loss that calculates the attenuation of signal strength over a distance, d is the distance, f is the frequency of the signal, and c is the speed of the signal propagation, which is the same as the speed of light.

2.4.2 Position Estimation with Known Distance

where the equation system intersects. The position can be calculated using the known position of the anchor nodes and the distance to the anchor nodes. If there are $n \geq 3$ anchor nodes, let $P = \begin{bmatrix} x \\ y \end{bmatrix}$ be the column vector of our desired positions. The location of the known anchors can be denoted as a matrix $A = \begin{bmatrix} x_1 & y_1 \\ x_2 & y_2 \\ x_3 & y_3 \\ \vdots & \vdots \\ x_n & x_n \end{bmatrix}$ and the distance as a vector $D = \begin{bmatrix} d_1 \\ d_2 \\ d_3 \\ \vdots \\ d_n \end{bmatrix}$ Then the residual can be calculated as $R_i = \sqrt{(A(i,1) - P(1))^2 + (A(i,2) - P(2))^2} - d_i$ where i represent up to the n-th anchor. Then the function can be combined and minimized using partial derivatives as shown in Equation 6. The result of this is the position were the equation system intersect.

$$\frac{\partial(x,y)}{\partial x} = \frac{\partial}{\partial x}\left(\sum_{i=1}^{n} R_i^2\right) = 2\sum_{i=1}^{n} R_i \frac{\partial R_i}{\partial x} = 0$$

$$\frac{\partial(x,y)}{\partial y} = \frac{\partial}{\partial y}\left(\sum_{i=1}^{n} R_i^2\right) = 2\sum_{i=1}^{n} R_i \frac{\partial R_i}{\partial y} = 0$$

Equation 6: partial derivative to find the point of intersection.

2.4.3 Serial Peripheral Interface (SPI)

The Serial Peripheral Interface (SPI) protocol facilitates synchronous serial communication between a master device and one or more slave devices. At its core, the SPI utilizes eight-bit serial shift registers embedded within the master and slave devices. Data transmission is orchestrated by a clock signal generated by the master device. When the master intends to transmit a byte of data to a slave, it loads the byte into its shift register. Subsequently, after eight clock pulses are generated, the slave retrieves the contents of the shift register, transferring each bit sequentially via the **M**aster **O**ut **S**lave **I**n (MOSI) line [10], [11].

Conversely, when data needs to be transmitted from the slave to the master, a similar process occurs utilizing the **M**aster **I**n Slave **O**ut (MISO) line. This results in an exchange of data between the respective shift registers of the master and slave devices, as shown in Figure 5.

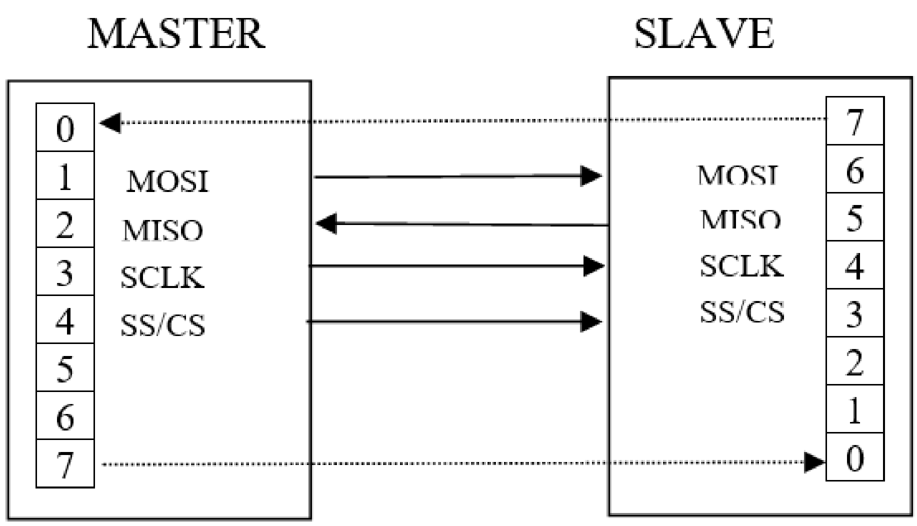

Figure 5. SPI with Master-Slave configuration

Notably, the SPI protocol accommodates communication with multiple devices by employing additional lines alongside MOSI and MISO. These lines, including the Chip Select (CS) line, enable the selection of specific devices for communication. When a master wants to talk to a particular slave, they use the SS (Slave Select) signal, with a low signal selecting the slave, as shown in Figure 6. The master coordinates data transfer timing through the Serial Clock (SCK) signal. To transfer data from the master to the slave, use the MOSI data line. Data is sent back to the master via the MISO data line from the slave. One or more slaves, each with its own Chip Select (SS) line, are typically connected to a master device via an SPI connection. By switching each slave's NSS line, the master can establish a one-to-one communication channel. Data is sent between the master and a selected slave in real-time in full-duplex mode, enabling simultaneous data transfer [10], [11].

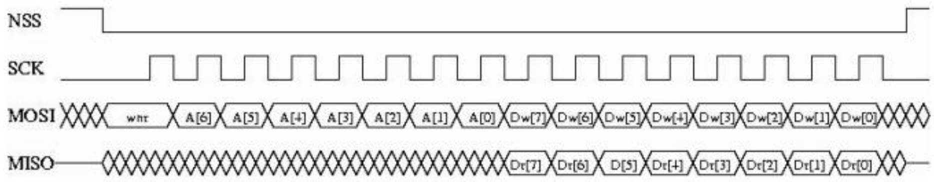

Figure 6. SPI communication protocol shows how the data is transmitted between the slave and master device. SCK is the serial clock, and MOSI is the data transmitted to the slave device; the first bit determines if it is a write/read operation, followed by the register to perform the operation on, and then lastly, the data to be transmitted, and if it's a read operation then the data is read from MISO line. This image is sourced from Sparkfun under the [Creative Commons Attribtion-NoDerivs 4.0]() International License, which permits unrestricted use, distribution, and reproduction in any medium, provided appropriate credit is given to the original creator.

SPI has no standard protocol and can be implemented with various voltage levels, such as 3.3V or 5V, which can be used based on the device's requirements and design. This flexibility allows them to adapt to different system voltage levels and device compatibility.

Users have the option to change the SPI protocol according to their needs. This determines the transfer order, speed, and clock frequency. Users can choose which SPI lines to use according to the device specifications. Users can configure SPIs to facilitate connection with various devices, such as sensors, memory chips, and other microcontrollers. SPI can be used in systems with many devices due to its versatility.

Clock polarity (CPOL) and clock phase (CPHA) settings pack data into fixed-length frames and control the precise data transmission timing. This flexible foundation mechanism enhances the protocol's adaptability to various applications and supports multiple data formats. One notable aspect of SPI is its capacity to concurrently support multiple slave devices, as shown in Figure 7. The master can selectively communicate with individual slaves by managing distinct chip select lines. This feature gives embedded systems the mobility to seamlessly process and coordinate many peripherals [10], [12].

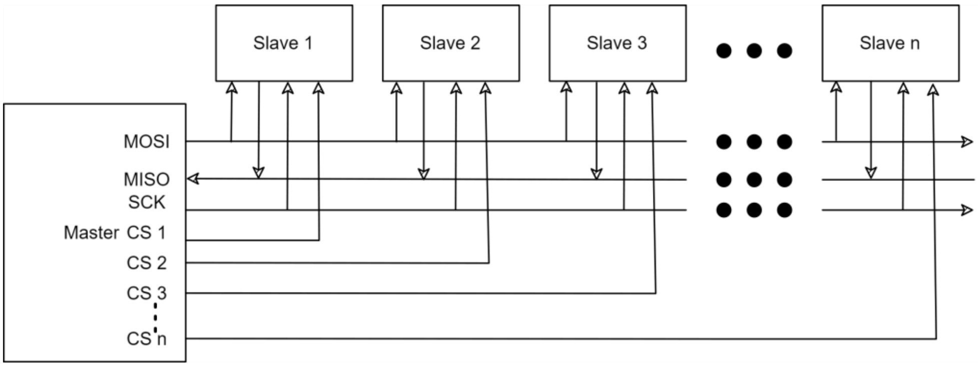

Figure 7. SPI master connected to multiple slaves.

2.4.4 P-Channel MOSFET

P-channel MOSFETs use holes instead of electrons as charge carriers. Gate (G), drain (D), and source (S) are its three terminals. A channel connects the source and drain within a P-doped region surrounded by a substrate having an N-doped content. The primary difference between enhancement and depletion types of P-channels MOSFETs is in their default state and how they respond to gate voltage. In Figure 8, there is a diagram illustrating both enhancement mode and depletion mode. When the gate voltage is at zero potential to the source, an enhancement-type PMOS is in the cutoff mode. A negative gate voltage is necessary to form a conductive channel, allowing current flow from the source to the drain. On the other hand, a depletion-type PMOS typically operates in the "on" state, conducting from source to drain when the gate voltage is zero. A positive gate voltage is necessary to deplete the channel and toggle the device off.

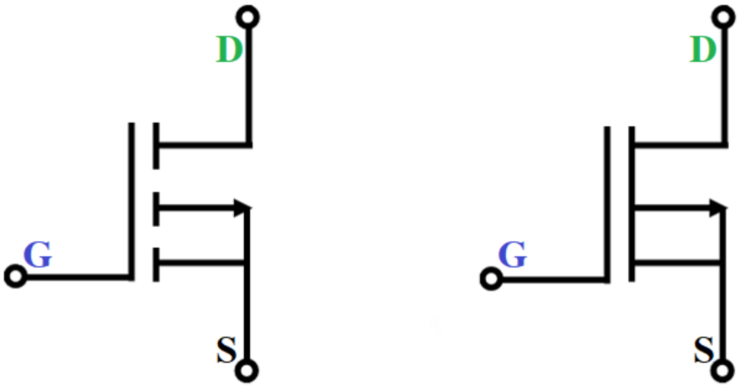

Figure 8. The diagram of enhancement-mode & depletion-mode PMOS

$$V_{GS} = V_G - V_S$$

Equation 7. V_{GS} is the voltage between the gate and source terminals.

Equation 7 shows the voltage between a P-MOSFET's gate and source terminals. Where V_G is the voltage at the gate terminal and V_S is the voltage at the source terminal. Both voltages are typically referenced to the same common ground or reference point. To turn on a P-channel MOSFET, V_{GS} should be negative and exceed the absolute value of the transistor's threshold voltage V_{th}.

2.4.5 NPN Transistor

NPN transistor is a type of bipolar transistor with two N-type and one P-type semiconductor materials fused; an NPN transistor is created. Three terminals are on an NPN transistor emitter, base, and collector. A positive current is biased at the base to drive an NPN transistor. This controls the flow of current from the collector to the emitter.

$$R_B = \frac{V_{BB} - V_{BE}}{I_B}$$

Equation 8. R_B is the base resistor in an NPN − transistor

Equation 8 calculates the base resistance, as shown in Figure 9, when the base-emitter voltage V_{BE} and the base current I_B are known. V_{BB} is the voltage applied to the base and V_{BE} is the voltage drop across the base-emitter, typically around $0.7V$ for silicon transistors.

$$R_C = \frac{V_{CC} - V_{LED}}{I_C}$$

Equation 9. R_C is the collector resistor in a transistor circuit.

Equation 9 is used to calculate the resistor for the collector R_C, its shown in Figure 9, where V_{CC} is the supply voltage in transistor circuits, V_{LED} is the voltage drop across an LED, I_C is the collector current in a transistor representing the flow of electrons from the collector to the emitter.

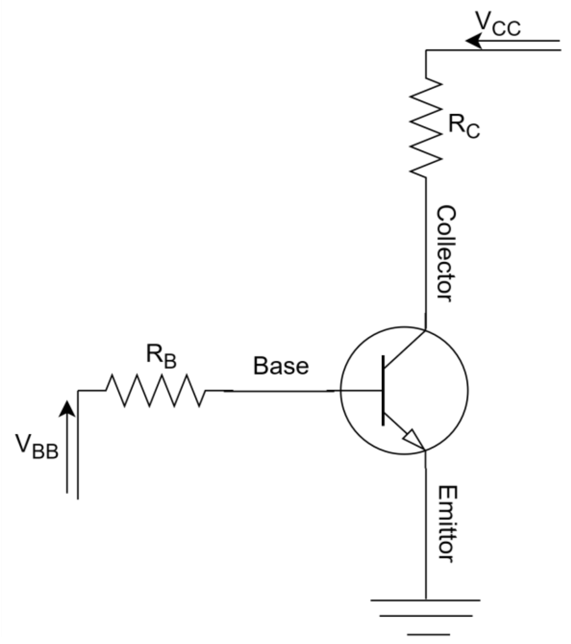

Figure 9. An NPN transistor with resistors in its collector R_C and base R_B

2.4.6 RFM69HCW

An extremely adaptable transceiver module, the RFM69HCW is utilized in many different wireless communications. Under various regulatory requirements, it can be used worldwide because it operates in the ISM (Industrial, Scientific, and Medical) frequency bands, usually at 315, 433, 868, or 915 MHz. This module is especially well-known for its long-range data transmission capabilities and low power consumption, which make it perfect for battery-operated devices and applications requiring long-range communication [13].

Support for configurable data rates up to 300 kbps and the option to use FSK (Frequency Shift Keying) or Ook (On-Off Keying) modulation techniques are among the technical specifications of the RFM69HCW. The capacity of this module to communicate over long distances without compromising data integrity is made possible by its high output power, which may reach up to +20 dBm, in conjunction with its sensitivity of -120 dBm at 1.2 kbps [14].

The RFM69HCW has several benefits, including its long-range capabilities, low power consumption, adaptability, and security features. Nonetheless, there are difficulties, like possible interference in the congested ISM band and the difficulty of overseeing vast networks of devices. These problems have been addressed with solutions such as adaptive frequency selection and mesh networking protocols, demonstrating the adaptability of the module and the active development community surrounding it.

2.4.7 Raspberry Pi Pico

Based on the Raspberry Pi RP2040 microcontroller chip, the Raspberry Pi Pico is a significant advancement in microcontroller boards. This advanced platform intends to provide professionals and enthusiasts with a versatile, robust, cost-effective embedded system project solution [15].

An ARM Cortex-M0+ dual-core CPU with a maximum clock speed of 133 MHz, the RP2040 chip powers the Raspberry Pi Pico. Because the RP2040 can process data simultaneously, it can handle more complex applications than its single-core competitors. With two cores, it can handle hardware connections with unmatched flexibility thanks to its programmable I/O (PIO) blocks, which have four state machines apiece. For multitasking and parallel processing in modern embedded systems, these characteristics make the RP2040 perfect.

Furthermore, 264 KB of SRAM, a notable feature compared to many microcontrollers in its class, makes the Raspberry Pi Pico stand out. Since working memory access needs to be dependable and quick, the SRAM's multi-bank architecture facilitates practical data storage and retrieval. The Raspberry Pi Pico is an excellent option for battery-powered and portable applications because its RP2040 processor minimizes power consumption while supporting high-capacity activities. Because of its powerful dual-core processor, rich programmable I/O capabilities, and large memory may be used for various applications, from IoT devices to educational tools [16-18].

3. Method

Various methods are available for indoor position estimation, each with strengths and limitations. The choice of hardware can restrict the range of feasible implementation methods. This section will primarily focus on an implementation utilizing signal strength indicators (RSSI) on Wi-Fi hardware, exponential regression, and the utilization of omnidirectional antennas using an embedded system on a custom-designed PCB.

3.1 Repurposing of Wi-Fi Hardware for RSSI-based Method

This technique leverages the usage of multiple APs that create multiple anchor nodes to ensure that the system is always at **L**ine **O**f **S**ight (LOS) with a minimum of 3 APs. The AP uses omnidirectional antennas to ensure the signal is transmitted equally in all directions. The distance can be calculated by reading the channel information signaling (CIS) and extracting the RSSI data [19].

3.1.1 List of Components

The components used in this part were the Raspberry Pi 5 and three access points of model Archer C20.

3.1.2 Implementation

This section will delve deeper into implementing trilateration techniques and 2D regression for achieving location estimation.

Beacon frames are a format of the IEEE 802.11 standard for Wireless Local Area Networks (WLANs), which are periodic signals broadcasted by APs. These frames serve as announcements, providing essential information about the network, such as the network's name (ESSID), supported data rates, encryption methods, MAC address, and other parameters. Devices within range, such as smartphones or laptops, passively listen for these beacon frames to discover and connect to available Wi-Fi networks. Additionally, beacon frames help devices maintain connectivity by providing synchronization information and allowing them to roam seamlessly between different access points within the same network.

The Raspberry Pi 5 utilizes the wireless chip BCM43455, a Single-Chip 5G WiFi IEEE 802.11ac MAC/Baseband/Radio with Integrated Bluetooth 4.1 and FM Receiver. This chip provides the RSSI from CIS and beacon frame information, accessed with the “iwlist wlan0 scan” command.

The RSSI information is obtained by scanning the surrounding network and obtaining beacon frames. The APs are programmed to broadcast beacon frames that contain the Extended Service Set ID (ESSID), where the location of the AP is encoded along with its identifier, which the receiver must check to ensure that the AP scanned belongs to the system. The identifier is a portion of the MAC address. When the receiver decodes this identifier, it compares it to the MAC address obtained through the beacon frame and thus confirms if that AP belongs to the system. This design choice was made to simplify adding new APs to the system. The scan uses the "iwlist" command, which grabs the beacon frame information scanned by the Network Interface Card (NIC) on the Raspberry Pi. This information is converted to a text format using the "subprocess" command; the program is executed as described in Figure 10.

In the previous section, 2.4.2, we introduced how location can be calculated using the distance information from three or more anchor nodes with known positions and distances to the receiver. However, this technique only partially suits our purpose because it requires exact distance measurements to calculate where the equation system intercepts. However, the core techniques of calculation remain the same. In our case, distances are estimated from the RSSI values, resulting in nonlinear equations for the anchor nodes with some uncertainty, thereby lacking a complete solution. 2D regression becomes crucial in finding a solution that closely fits the equation system.

The trilateration process, as implemented in the function "trilaterate" (refer to Appendix 1 for detailed implementation), operates by utilizing anchor information, which comprises the precise positions of anchors along with their estimated distances. Initially, a reference position is established, typically set at the origin. The objective is to iteratively adjust this reference position towards the target position that is to be estimated. This iterative adjustment minimizes the residual, representing the disparity between the distances from the reference position to the anchors and the estimated distances from the receiver to the anchors. The residual is computed in each iteration, reflecting the difference between the reference position, the anchors, and the estimated distances.

Given a system of linear equations Ax = b where A is a matrix representing the coefficients and is the vector of the target, the goal is to find the vector x that minimizes the squared Euclidean norm of the residual r = b - Ax. This minimization can be expressed as $x = argmin_x||b - A_x||^2$, this is solved with the Least square method which minimizes the Euclidean norm of the residual expressed as $(A^TA)^{-1}A^Tb$ where A^T is a transpose matrix of matrix A and $(A^TA)^{-1}$ is the inverse of the matrix A^TA.

In practice, directly computing the $(A^TA)^{-1}$ can be numerically unstable and computationally expensive, especially for large matrices. Instead, the “np.linalg.lstsq” function computes the solution using the Singular Value Decomposition (SVD) method, which is more numerically stable and efficient. The SVD method decomposes matrix A into three matrices U, Σ, and V^T such that $A = U\Sigma V^T$. The solution x can be computed using the decomposition $x = V\Sigma^{-1}U^T b$. This method can handle instances where the matrix is ill-conditioned or non-invertible.

The least squares method then determines the adjustment needed to bring the reference position closer to the estimated position. This adjustment is based on the Jacobian matrix, which encapsulates the sensitivity of the residuals to changes in the reference position. Subsequently, the reference position is updated according to this adjustment, and the process continues until convergence or until a specified maximum number of iterations is reached.

It's important to note that an offset is applied to the anchor position to prevent division by zero errors in linear regression. If an AP were positioned at the origin, this would result in a residual of 0 when calculating the distance to the first reference position. This offset, subtracted from the result, ensures numerical stability throughout the process.

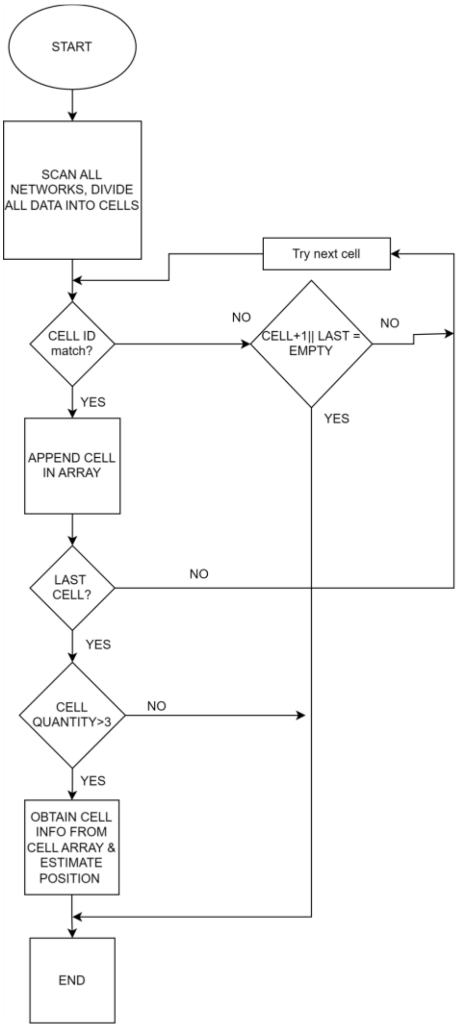

Figure 10. Program structure for position calculation with multiple AP.

3.1.3 Testing

Testing was conducted in a room approximately 5 meters by 8 meters (see Appendix 2). Access points (APs) were positioned half a meter from the walls. Six positions were designated within the room for location measurements. The APs were programmed to transmit their predetermined positions periodically. Initially, AP1 was placed at the origin, and the other APs were positioned at coordinates (300,0) and (300,600).

To collect measurements, the receiver was taken to each predetermined position. Upon reaching each location, the trilateration algorithm was initiated by pressing a button. This algorithm estimated the current position and saved the data to a corresponding file. The process was then repeated for the remaining positions, with the receiver relocated each time. This entire procedure was iterated 26 times, producing 156 measurements.

The Root Mean Square Error (RMSE) is a statistical tool that measures the average deviation between estimated values and actual values in a dataset. It calculates the square root of the average squared differences between estimated and actual values, providing a single number to gauge the accuracy of a predictive model, see Equation 10. A lower RMSE indicates better estimation performance, with zero representing a perfect match between estimated and actual values. The error between the actual and estimated positions is the distance between these two values. This means that the error in RMSE is calculated using the distance formula.

$$RMSE = \sqrt{\frac{1}{n}\sum_{i=1}^{n}(x_{actual} - x_i)^2 + (y_{actual} - y_i)^2}$$

Equation 10: RMSE reduced function, n is the number of measurements of the estimated positions in the dataset.

3.2 RFM69HCW and RP2040

The Raspberry Pi 5 utilizes a PCB antenna, as shown in Figure 11. According to Lai H and Wong H [19], this dipole PCB antenna has no complete omnidirectional radiation pattern. This is crucial to achieve a more precise RSSI reading in all directions. We looked into a dedicated transceiver where a monopole antenna can be utilized to achieve more accurate measurements.

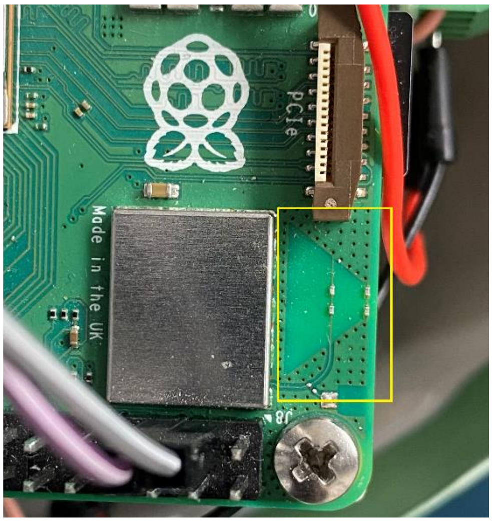

Figure 11: A portion of the Raspberry Pi PCB with the PCB dipole antenna marked in yellow.

3.2.1 List of Components

The components mentioned in our Bill of Materials from OrCAD apply to one board, and we have two circuit boards.

Table 1. All the components used during the design of the embedded transceiver.

Item	Quantity	Reference	Part
1	3	D1,D2,D3	LED_LAMPA
2	1	D4	Diod
3	1	J1	PWR Connector
4	2	K1,K2	Knapp
5	3	Q1,Q2,Q3	NPN
6	2	Q4,Q5	PMOS
7	7	R1,R2,R8,R9,R10,R11,R12	
8	2	R3,R4	
9	3	R5,R6,R7	
10	1	U1	RPI PICO
11	1	U2	RFM69HCW
12	1	U3	ANTENN

3.2.2 PCB Design

In our design, three LEDs were required to indicate the different program states running on the RPP. Running these LEDs individually directly from the RPP is possible because each LED draws about 20mA current. However, according to the datasheet for the RP2040 processor [20, p. 619], the sum of all current being sourced by GPIO is 50 mA. This means that if all three LEDs are required to be on, the GPIO cannot supply the current needed. This led us to design the LEDs to be driven from other sources, in this case, either the battery power or the 3v3 pin on RPP, which, according to the datasheet, can supply up to 300mA [21, p. 8].

According to the datasheet for the red diode, the typical forward voltage is approximately 2.4V, with a forward current capacity of 20mA [22]. To calculate the resistance in the collector of the transistor that was used to activate the LED, we use Equation 9. The voltage from the V_{CC} is 3.3V, connected to the collector as shown in Figure 12.

$$R_C = \frac{V_{CC} - V_{LED}}{I_C}$$

$$R_C = \frac{3.3 - 2.4}{20 * 10^{-3}} = 45\Omega$$

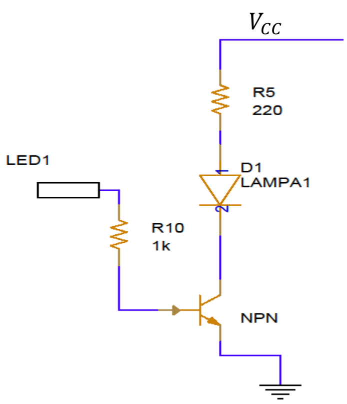

Figure 12. A led-activation circuit using an NPN transistor by a signal from a microcontroller.

We now continue to calculate the collector's resistance for the green diode. According to the datasheet for the green diode, the typical forward voltage is approximately 2V, with a forward current capacity of 20mA[23], which uses the same Equation 9 used for the red diode.

$$R_C = \frac{3.3 - 2}{20 * 10^{-3}} = 65\Omega$$

We used the same Equation 9 to calculate the resistance in the collector with a blue diode, and according to the blue diode datasheet, the typical forward voltage is 3.2V, with a forward current capacity of 15mA [24].

$$R_C = \frac{3.3-3.2}{15*10^{-3}} = 7\Omega$$

Finally, we used Equation 8 to calculate the R_B resistance shown in Figure 12. 3.3Vis the input voltage V_{BB} and 0.7 is the base-emitter voltage V_{BE}. According to the datasheet, the transistor is driven in saturation region with a current of 2 mA, which results in a voltage drop of 0.18 volts on V_{CE} which is an insignificant change in our goal to drive the LED.

$$R_B = \frac{3.3-0.7}{2*10^{-3}} = 1300\Omega$$

3.2.3 Impedance Matching and Coplanar Waveguide

In electronic design, impedance plays a pivotal role in power transfer. It comprises two components: resistance (the real part) and reactance (the imaginary part), which stems from capacitance and inductance. Represented as Z = R + jX, where j is the imaginary unit, impedance matching dictates how effectively energy flows from a source circuit (Zs) to a load (Zl), depicted in Figure 13. According to the maximum power transfer theorem[25] the impedance of the load must be the same as the impedance of the source to maximize the power transfer.

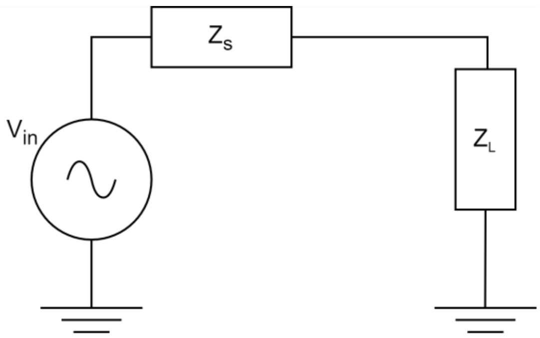

Figure 13. The circuit diagram with Z_L and Z_S.

For instance, as in our study, ensuring impedance matching is crucial when designing a transmission line. Any discrepancy between transmitter and receiver impedance leads to reflections, quantified by the reflection coefficient Γ(gamma). To mitigate reflections, Z_L needs to match Z_S see Equation 11.

$$\Gamma = \frac{Z_L - Z_S}{Z_L + Z_S}$$

Equation 11. Reflection coefficient in transmission line

The RFM69HCW module lacks a pre-installed antenna, so the transmission line configuration requires manual setup. Following the datasheet's guidance, we aimed to maintain a 50-ohm impedance for the transmission line to the antenna. Achieving this necessitated employing a coplanar waveguide (CPW) to accurately determine the transmission line's impedance. CPW is a type of surface-strip transmission line that can be fabricated on a PCB [26] and consists of a transmission line surrounded by a ground plane on both sides of the substrate material see Figure 14.

CPW offers advantages over other transmission lines due to its geometry, where all conductive elements lie on the same plane. This geometric simplicity facilitates impedance calculations, streamlining the design process for optimal performance, as described in Equation 12.

$$Z_{CPW} \approx \frac{60}{\sqrt{\varepsilon_{eff}}} \frac{ln(\frac{8S}{W} + \frac{W}{4G})}{\sqrt{1 + 12\frac{H}{G} - 0.5ln(\frac{4\pi W}{G})}}$$

Equation 12: ε_eff is the effective dielectric constant of the substrate material. W is the width of the conductor strip. H is the height of the substrate. G is the space width between the conductor strip and the ground plane.

AppCAD is an application tool that facilitates the calculation of transmission line impedance. This application was utilized to calculate the correct size and length of the transmission line on the PCB printed on FR4 substrate to achieve a 50-ohm impedance. The application takes in variables, as shown in Figure 14, then the impedance is calculated, and adjustments are made to reach the target impedance.

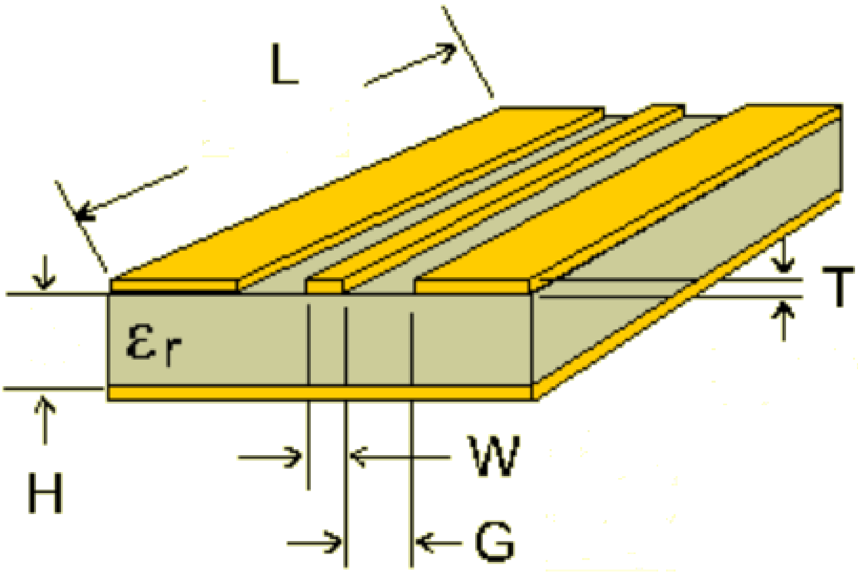

Figure 14.CPW transmission line. W is the width of the conductor strip. H is the height of the substrate. G is the space width between the conductor strip and the ground plane. This image is sourced from AppCad under [© 1989–2008 Avago Technologies] copyright. All rights reserved. Redistribution without modification is permitted. See license for details.

3.2.4 Power Selector

The circuit primarily relies on USB power and allows battery operation through a modular design. However, introducing a battery to the RPP that powers the entire circuit presents challenges, particularly when the USB is also connected for programming. This dual power source scenario may lead to issues such as reverse currents see Figure 15. The figure shows how the power components in the RPP are connected, and we can see that no diode is used for reverse current protection into VBUS or 3v3 pin. No protection exists from powering the circuit with two power supplies. To address this concern, a protection circuit was designed to ensure that the RPP and external circuit operate on a single power supply, even when both power sources are connected.

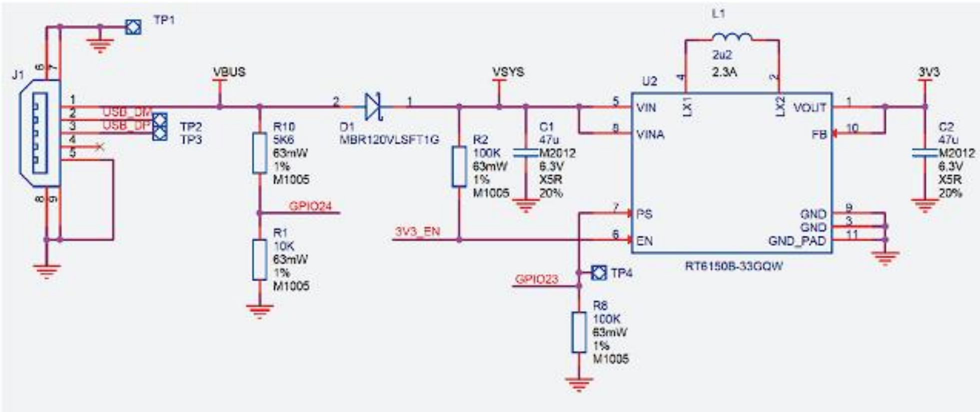

Figure 15: The power circuit of the Raspberry Pi Pico. This image is sourced from the Raspberry Foundation under the [Creative Commons Attribtion-NoDerivs 4.0](#) International License, which permits unrestricted use, distribution, and reproduction in any medium, provided appropriate credit is given to the original creator.

In this circuit Appendix 5, two P-channel metal-oxide-semiconductor field-effect transistors (PMOSFETs) operating in depletion mode were utilized. The first transistor detects the presence of power from the USB, effectively shutting off to prevent the battery from powering the circuit simultaneously. The second transistor prevents the external circuit from being powered by the battery while the 3.3V from the RPP is active. This is crucial because the 3.3V line connects with the VSYS, the pin that powers the RPP from an external source. If the USB is connected and the 3.3V line powers the external circuit, there's a risk of power feeding back into the VSYS, potentially causing internal damage to the RPP.

To mitigate this risk, a diode is integrated to ensure unidirectional current flow, preventing current back-feeding into the VSYS. This arrangement ensures that power flows only from the designated source to the circuit, maintaining system integrity and avoiding damage to sensitive components.

3.2.5 The RFM69HCW Driver

The RFM69HCW module is a transceiver with pre-existing drivers tailored for platforms featuring Atmega processors. However, developing custom drivers becomes necessary if one utilizes it with an alternative processor.

Our decision to adopt the RP2040 stems from its cost-effectiveness and significantly lower power consumption than its Atmega counterparts. This forced us to develop a new driver that allows the transceiver to operate with the RP2040 processor. Leveraging the SPI protocol for communication, we created a driver using the C++ programming language, enabling seamless interaction between the RP2040 and the RFM69HCW module. Using the SPI protocol meant that we had to program the RP2040 processor to send a signal to the SPI bus with the same characteristics as the Atmega processor; this means that we could reuse the same methodology recommended by the RFM69HCW provider for communication.

Furthermore, the RFM69HCW uses a line from pin D0 while configured in communication mode to signal the processor when the received data is ready by setting the pin to high and back to low once the data has been read from the RECEIVED_DATA_READY register. When developing the driver, that had to be considered; the line D0 was connected to a general-purpose **input-output** pin on the RP2040. The polling technique was used; the processor would utilize one of its cores to check if the data was ready and then configure the transceiver into read mode to let the processor read the register's content. Additional circuits were added to facilitate debugging; these buttons let us change into other modes of choice, and LED lights indicate which mode the program operates.

3.2.6 Testing the Embedded System

We carefully checked each component's functioning during testing to ensure it complied with the criteria. We confirmed the stability and dependability of the communication link between the modules by sending and receiving packets. To determine the system's power consumption under different operating conditions, we simultaneously kept a tight eye on the current meter.

Despite thoroughly testing the transmitter and receiver to ensure appropriate performance, we could not test location estimation using the trilateration algorithm in 3.2.6. This component is essential since our thesis aims to create a position finder. Regretfully, our options were limited by the ability to acquire more RFM69HCW modules, which are necessary for performing trilateration accurately enough. We could only acquire two modules, even though we tried to obtain more.

To verify that external components work correctly and integrate with our system, it is crucial to mention that the main focus of our testing was to validate driver routines. Ensuring that our position finder functions accurately and dependably in real-world scenarios is contingent upon extensive testing. Notwithstanding the absence of trilateration-based position testing, our test findings have improved comprehension of the functionality and performance of the system and highlighted any areas that require further development in subsequent project cycles.

3.3 Intellectual Property Statement on Embedded System Development

The GNU General Public License version 3(GPLv3) contains the integration permission and recommendations. We can use, modify, and share the code because of the GPLv3 license. Furthermore, GPLv3 guarantees that our derivative works are free to use and bound by the same license conditions.

The development of the RFM69HCW driver stems from the driver already developed for the ATMEGA processor utilized in the Arduino environment; due to the incompatibility of the processor structure, we were forced to build our drivers with the main inspiration from the drivers already provided.

Following SparkFuns copyright policies, compliant with GPLv3, is a testament to our dedication to the open-source community. The community is encouraged to share information and work tighter to improve things, and these policies permit the usage and modification of already-existing materials. With code distributed under these terms, we ensure our contribution is morally and legally sound, promoting growth and innovation in the embedded systems programming community.

4. Results

This section shares the project's results for creating a system for indoor positions. Our system is designed to facilitate indoor position estimation and allow the system to be implemented more efficiently for future use.

4.1 Results for RSSI Method

We gathered 150 data, carefully measuring the relationship between distance (cm) and signal strength (dBm). This was done manually by measuring the distance using a measuring tape and recording the RSSI value extracted from CIS. To analyze this, we used a statistical method called the least squares method. In section 2.4.1, we discussed why the characteristic of this function is exponential, which is why an exponential regression was chosen. This helped us process the data and drive a mathematical equation summarizing the relationship between the RSSI value and distance.

Following the application of the least squares method, an exponential equation was obtained, as illustrated in Figure 16 (highlighted in blue). This equation serves as the primary foundation for constructing an intricate model explaining the influence of distance on signal strength, referred to as Equation 13, and serves as a guide in comprehending the complex relationship between these variables.

$$y = e^{2.59431-0.0815715x} = 13.3873469 * e^{-0.0815715x}$$

Equation 13. The equation shows the relationship between distance (y) and signal strength (x). This is only applicable to the hardware used in this work.

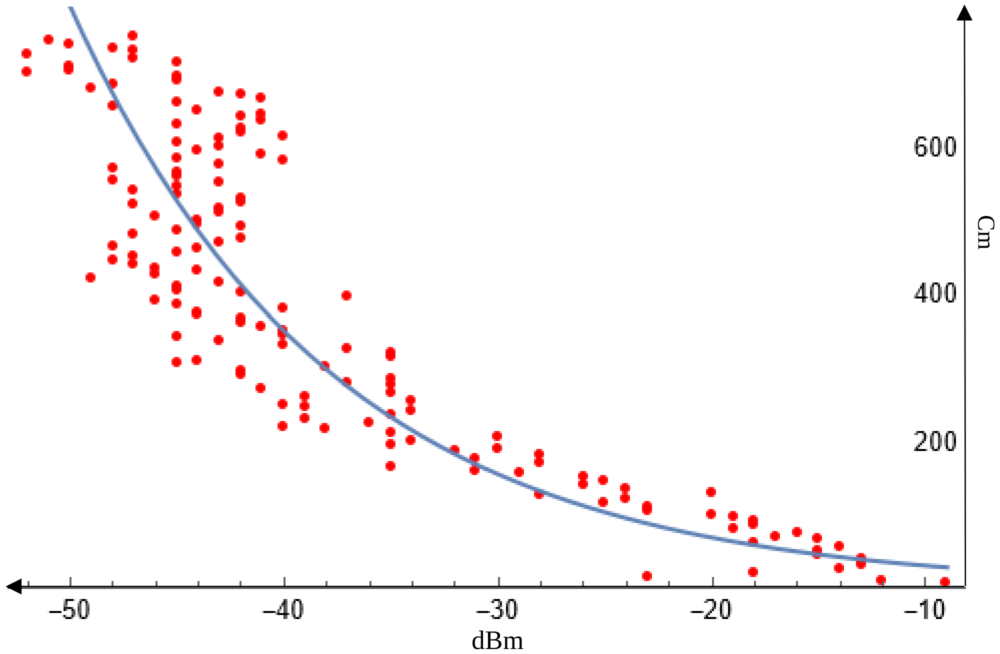

Figure 16. The data measured. The y-axis represents the distance between the AP and the receiver measured in cm, and the x-axis is the signal strength value measured in dBm. The line is a function that fits the measured data best.

4.1.1 Position in the Room

Figure 17 shows a detailed scatter plot including 156 data points, which chart the positional readings recorded by our trilateration algorithm. At the forefront are six distinctly marked points, labeled position 1 to position 6. These are the standard positions that serve as reference points in our system's dataset, providing a baseline for the accuracy of the positioning data.

The scatterplot shows the system's ability to function across various conditions and moments. The dots are distinct colors, and each color represents different data from the 6 distinct reference points. The dots are the measured points, and their color connects them to their reference point.

There are three APs strategically placed in the room, and these are the anchor points utilized for position estimation. To calculate the system's accuracy, all measured points were divided by all measured points in the room. The measured accuracy is 71.654%.

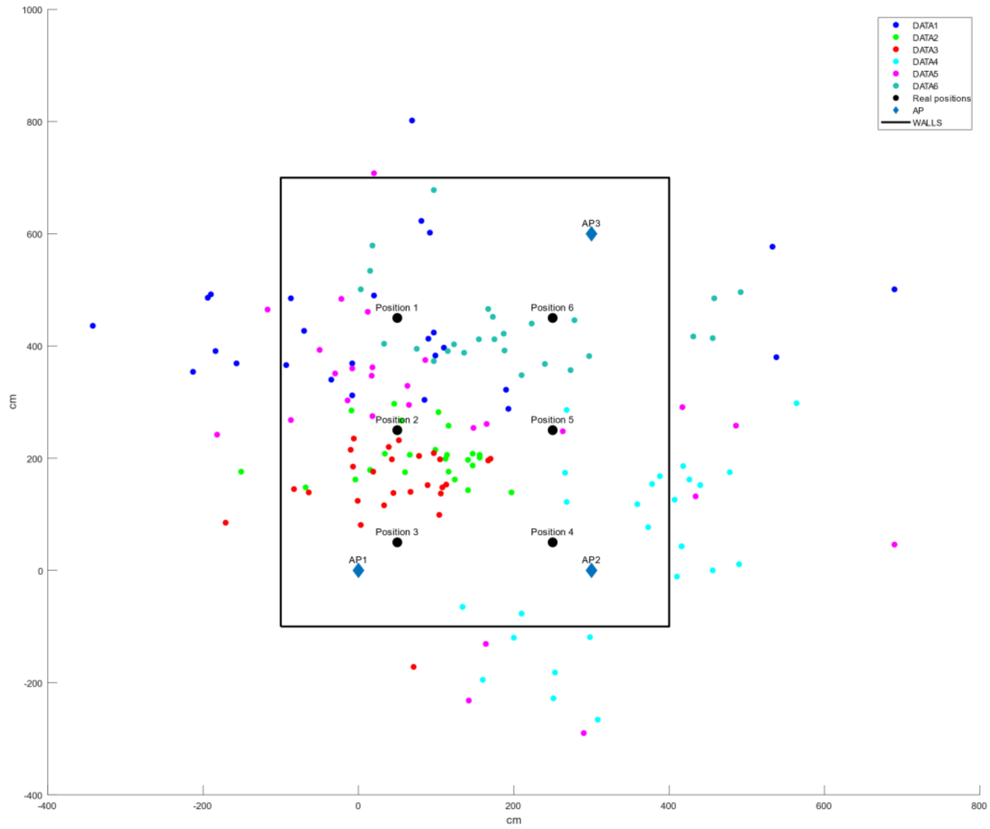

Figure 17. The results of the estimated position in the room, positions 1-6, show the reference positions; the data are the corresponding estimate to those positions.

We calculate the RMSE value for the six actual points, which informs us about the accuracy of our measured data, as shown in Figure 18. From this data, we can calculate the mean value of the RMSE 202 cm.

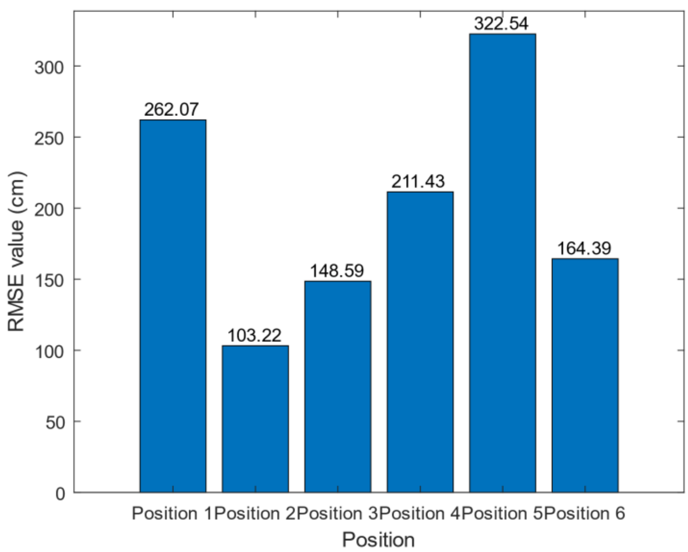

Figure 18. The value of RMSE for six different positions.

4.2 Result of the RFM69HCW Design.

The PCB design was achieved using Allegro-ORCAD software, showcasing a comprehensive arrangement of electrical components. For detailed insights into the component layout, please refer to Appendix 4 and Appendix 5.

The final design was then manufactured using the milling method, where fabrication utilized a double-sided FR-4 substrate; the component was then soldered on to produce the result presented in Figure 19.

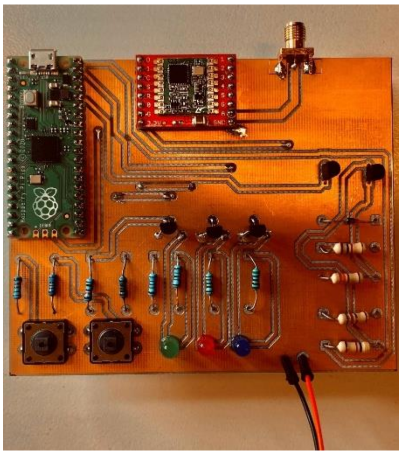

Figure 19. The PCB with all its components soldered on.

To ensure accurate impedance determination for our transmission line, we've employed coplanar waveguide techniques to determine the desired width of the transmission line. Figure 20 shows the measurements of the transmission line width at approximately 2.1 mm, which is close to our desired 2.23 mm. It's possible to measure the impedance more precisely with the help of a Network Vector Analyzer (VNA); however, this is not a standard tool we can get hold of.

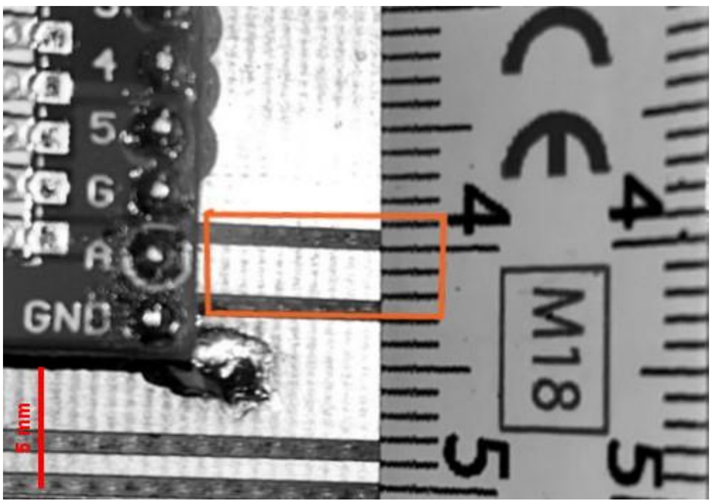

Figure 20. width of the transmission line.

5. Discussion

Through this research, improved indoor navigation systems are being investigated, highlighting the challenges and opportunities associated with utilizing both dedicated RFM69HCW transceivers and repurposed Wi-Fi infrastructure. Nuanced insights on the practicality, difficulties, and implications of these approaches for the future of indoor navigation technology were obtained from our inquiry.

Although the current Wi-Fi infrastructure offers an inexpensive and easily accessible resource for indoor positioning, our research shows that the fluctuating signal strength causes substantial obstacles. The application of RSSI brought to light the dynamic character of interior spaces and the critical role that environmental elements play in determining signal propagation. Despite these challenges, the least squares approach used to create equations has shown that statistical modeling can provide some predictability and reliability to RSSI-based locations, even though consistency and precision are limited.

Indoor navigation took on a new dimension by investigating RFM69HCW transceivers for dedicated device localization. Tailored solutions for indoor positioning systems are feasible, as demonstrated by creating a PCB and drivers that connect the Raspberry Pi Pico (RPP) and the transceiver. However, the restricted availability of RFM69HCW modules limited the project's scope. It made it more difficult to thoroughly test and evaluate the suggested trilateration algorithm tested with the Wi-Fi method. This restriction underlines the need for scalable and easily accessible solutions to advance indoor navigation technology and the practical difficulties associated with hardware-based research.

5.1 Comparison With Other Works

In section 2.2, a related study that has been of interest is mentioned. The focus is on positioning and navigation:

The “ALRD: AoA Localization with RSSI Differences” [3] project discussed the ALRAD positioning method, combining RSSI and AoA with quadratic and linear regression analyses. This approach involves specially aligned antennas to predict RSSI values from various angles to enhance positioning accuracy. The method reduced the average localization error on an indoor setting from 124 cm per square meter to 89 cm, a reduction of about 29%, by employing techniques to collect signal data for accurate position estimation densely.

Our project explores indoor navigation by leveraging existing Wi-Fi infrastructure. This method approach allowed for a comprehensive examination of indoor positioning accuracy by utilizing the strength of wireless technologies. We achieved the lowest RMSE value of 103.22 cm, and the highest was 322.54 cm for our six positions. Subsequently, we calculated the average, which was 202 cm. However, the ALRD achieved significantly better results than we did due to their combination of two methods: RSSI with least squares method and AoA, which led to enhanced outcomes and improved precision. Another factor could be the choice of hardware. Our implementation was heavily influenced by the affordability of the hardware, which led to the selection of hardware without the desired radiation pattern.

6. Conclusion

The interface of RP2040 processors with RFM69HCW transceivers proved to be a substantial issue, requiring new drivers. Compatibility and communication protocols can become significant obstacles when merging disparate technology, and this challenge was representative of more general problems in this regard. Furthermore, the indoor environment posed a considerable challenge due to physical barriers and multipath effects that complicated signal-based location techniques. The difficulties highlight the intrinsic intricacy of interior navigation systems and the necessity for diverse resolutions.

The project results highlight how crucial it is to keep up with advancements and studies in indoor navigation. Future research should investigate hybrid techniques integrating several technologies and sensors to alleviate the constraints noted in RSSI variability. For example, adding inertial measurement units (IMUs) could compensate for the shortcomings of signal-based techniques, providing more reliable and precise positioning.

Furthermore, this initiative offers a promising path for sustainable technology growth because it focuses on recycling electronic waste for indoor navigation. To better integrate technical breakthroughs with environmental sustainability goals, future initiatives could expand the scope of this approach to include a broader range of devices and components.

The present study adds to the dynamic field of indoor navigation technology by shedding light on the advantages and disadvantages of innovative methodologies. This initiative improves indoor navigation technology and encourages a more comprehensive approach to sustainability in technology development by pushing the limits of what can be achieved using reused and dedicated gear.

In conclusion, this study has opened many avenues for further research, even as it has established a solid platform for investigating novel approaches to indoor navigation. The future stages in this fascinating topic will depend critically on addressing the issues found and utilizing the knowledge acquired. Developing accurate, dependable, and sustainable indoor navigation systems is attainable with sustained innovation and interdisciplinary cooperation.

7. References

[1] “ERC Recommendation 70-03,” 2014.

[2] G. Blewitt, “Basics of the GPS Technique: Observation Equations §,” 1997.

[3] J. R. Jiang, C. M. Lin, F. Y. Lin, and S. T. Huang, “ALRD: AoA localization with RSSI differences of directional antennas for wireless sensor networks,” *Int J Distrib Sens Netw*, vol. 2013, 2013, doi: 10.1155/2013/529489.

[4] J. Dong, M. Noreikis, Y. Xiao, and A. Ylä-Jääski, “ViNav: A Vision-Based Indoor Navigation System for Smartphones,” *IEEE Trans Mob Comput*, vol. 18, no. 6, pp. 1461–1475, Jun. 2019, doi: 10.1109/TMC.2018.2857772.

[5] T. H. Riehle, P. Lichter, and N. A. Giudice, “An indoor navigation system to support the visually impaired,” in *2008 30th Annual International Conference of the IEEE Engineering in Medicine and Biology Society*, 2008, pp. 4435–4438. doi: 10.1109/IEMBS.2008.4650195.

[6] V. Lazarev, G. Fokin, and I. Stepanets, “Positioning for Location-Aware Beamforming in 5G Ultra-Dense Networks,” in *2019 IEEE International Conference on Electrical Engineering and Photonics (EExPolytech)*, 2019, pp. 136–139. doi: 10.1109/EExPolytech.2019.8906825.

[7] A. U. Ahmed, R. Arablouei, F. de Hoog, B. Kusy, R. Jurdak, and N. Bergmann, “Estimating angle-of-arrival and time-of-flight for multipath components using wifi channel state information,” *Sensors (Switzerland)*, vol. 18, no. 6, Jun. 2018, doi: 10.3390/s18061753.

[8] M. Schüssel, “Angle of Arrival Estimation using WiFi and Smartphones,” 2016.

[9] A. Pal, “Network Protocols and Algorithms Localization Algorithms in Wireless Sensor Networks: Current Approaches and Future Challenges Network Protocols and Algorithms,” 1943. [Online]. Available: www.macrothink.org/npa45

[10] A. N, G. Joseph, S. S. Oommen, and R. Dhanabal, “Design and implementation of a high speed Serial Peripheral Interface,” in *2014 International Conference on Advances in Electrical Engineering (ICAEE)*, 2014, pp. 1–3. doi: 10.1109/ICAEE.2014.6838431.

[11] S. C. DHURY, G. K. SINGH, and R. M. M. HRA, “Design and Verification Serial Peripheral Interface (SPI) Protocol for Low Power

Applications," *Int J Innov Res Sci Eng Technol*, vol. 03, no. 10, pp. 16750–16758, Oct. 2014, doi: 10.15680/ijirset.2014.0310048.

[12] I. I. bin Jamaludin and H. binti Hassan, "Design and Analysis of Serial Peripheral Interface for Automotive Controller," in *2020 IEEE Student Conference on Research and Development (SCOReD)*, 2020, pp. 498–501. doi: 10.1109/SCOReD50371.2020.9250981.

[13] H. Wang, M. Ouyang, Q. Meng, and Q. Kong, "A traffic data collection and analysis method based on wireless sensor network," *EURASIP J Wirel Commun Netw*, vol. 2020, no. 1, Dec. 2020, doi: 10.1186/s13638-019-1628-5.

[14] A. S. Ali, C. Coté, M. Heidarinejad, and B. Stephens, "Elemental: An open-source wireless hardware and software platform for building energy and indoor environmental monitoring and control," *Sensors (Switzerland)*, vol. 19, no. 18, Sep. 2019, doi: 10.3390/s19184017.

[15] V. Harvey, "Title: Automated device for Raspberry Pi Pico recovery Number of Pages: 32 pages + 2 appendices," 2023.

[16] A. Pal, "Localization algorithms in wireless sensor networks: Current approaches and future challenges.," *Netw. Protoc. Algorithms*, vol. 2, no. 1, pp. 45–73, 2010.

[17] D. Loker, "Embedded Systems using the Raspberry Pi Pico," in *2022 ASEE Annual Conference & Exposition*, 2022.

[18] Y. Yang MEng Field Advisor, V. Hunter Adams, and B. Robert Land, "DESIGNING A CAMERA MODULE DRIVER USING PROGRAMMABLE I/O ON PI PICO RP2040 A Design Project Report," 2022.

[19] A. Pal, "Network Protocols and Algorithms Localization Algorithms in Wireless Sensor Networks: Current Approaches and Future Challenges Network Protocols and Algorithms," 1943. [Online]. Available: www.macrothink.org/npa45

[20] Raspberry Pi Foundation, "RP2040_datasheet." Accessed: Mar. 18, 2024. [Online]. Available: https://datasheets.raspberrypi.com/rp2040/rp2040-datasheet.pdf

[21] Raspberry Pi Foundation, "pico-datasheet", Accessed: Mar. 19, 2024. [Online]. Available: https://datasheets.raspberrypi.com/pico/pico-datasheet.pdf

[22] Multicomp, "Datasheet Red LED, MV5754A." Accessed: Apr. 18, 2024. [Online]. Available: https://www.farnell.com/datasheets/1498852.pdf

[23] KingBright, “Datasheet Green LED, rlL_7113GD.” KingBright. Accessed: Apr. 18, 2024. [Online]. Available: https://media.distrelec.com/Web/Downloads/ta/_e/rlL-7113GD_data_e.pdf

[24] KingBright, “Datasheet Blue LED, L-9294QBC-D.” Accessed: Apr. 18, 2024. [Online]. Available: https://docs.rs-online.com/2b8e/0900766b8139d764.pdf

[25] C. S. Kong, “A general maximum power transfer theorem,” *IEEE Transactions on Education*, vol. 38, no. 3, pp. 296–298, 1995, doi: 10.1109/13.406510.

[26] C. P. Wen, “Coplanar Waveguide: A Surface Strip Transmission Line Suitable for Nonreciprocal Gyromagnetic Device Applications,” *IEEE Trans Microw Theory Tech*, vol. 17, no. 12, pp. 1087–1090, 1969, doi: 10.1109/TMTT.1969.1127105.

8. APPENDIX

Appendix 1: Trilateration Algorithm for Wi-Fi

```
import subprocess
import time
import math
import numpy as np
import re
import gpiod

#scanning button and indicator when scanning
led_pin = 12
button_pin = 16

""" Scan nearby network and retreive info,RSSI, SIgnal quality, Mac-
adress..., osv"""
def scan_all_networks():

    try:
        # Run the iwlist command to scan for Wi-Fi networks
            result  =  subprocess.check_output(["sudo","iwlist","wlan0",
"scan"], universal_newlines=True)

       ''' Split the output into individual cells, these cells correspond
information for each nearby AP '''
        cells = result.split("Cell ")
        return cells
    except subprocess.CalledProcessError as e:
            print("Error running iwlist: {}".format(e))

"""Check if the AP scanned bellongs to the system"""
def checkID(cells):

    cell_info = cells.split("\n")
    ESSID, = re.findall(r'ESSID:"(.*?)"',cell_info[5])
    MAC, = re.findall(rf'{re.escape("Address:")}\s*(.*)',cell_info[0])
    if ESSID.startswith("TN"):
        last2f1 = ESSID[-2:]
        last2f2 = MAC[-2:]
        if last2f1 == last2f2:
            return True
        else:
            return False

"""append cell info to a list"""
def append_cells(cells):
    Node_cell = []
    for cell in cells[1: ]:
        if checkID(cell):
            Node_cell.append(cell)
    return Node_cell


def position_estimate(Node_cell):

    #here three node info will be saved, xpos, ypos, distance
```

```
    Node_info = []

    """extracting info from the cells"""
    for cell in Node_cell[0: ]:
        cell_info = cell.split("\n")
        stringdata = cell_info[3]
        index = stringdata.find("Signal level=")
        signal_data = stringdata[index + len("Signal level="):]
        signal_data = re.findall(r"[-+]?\d*\.\d+|\d+", signal_data)

        #formula for conversion from signal strength to centimeter
       distance = math.exp(2.59431-(0.0815715*(-float(signal_data[0]))))

        #extracting position info for the node
        ESSID, = re.findall(r'ESSID:"(.*?)"',cell_info[5])
        posx = ESSID[-10:-6]
        posy = ESSID[-6:-2]
        Node_info.append([posx,posy,distance])

    Node_info = np.array(Node_info)
      init_guess  =  np.array([0.0,0.0])  '''the  reference  point  for
calculation using the lsq method '''


    return trilaterate(Node_info,init_guess)


''' this function estimate the position of a device, from n anchors//AP
position and distance data using linear regression '''
def trilaterate(anchors, initial_guess):
    position = initial_guess.copy()
    max_iterations = 100
    tolerance = 1e-6

'''maximum iteration to make more precise estimation with lsq method,
more iteration means precise estimation but also takes longer to compute
'''
    for _ in range(max_iterations):

        residuals = []'''residual for the difference between the anchor
nodes and the actual position sqr((x-xn)²+(y-yn)²)-d '''
        lsqmat = [] #matrix to compute the lsq method

        for anchor in anchors[0:]:
            anchor = [float(num) for num in anchor]

            # the distance from origo to the ancher nodes
                d  =  np.sqrt((position[0]  -  float(anchor[0]))  **  2  +
(position[1] -float(anchor[1])) ** 2)
            residuals.append(d - float(anchor[2]))

            # Jacobian matrix
            lsqmat.append([
                (position[0] - anchor[0]) / d,
                (position[1] - anchor[1]) / d
            ])
```

```
        residuals = np.array(residuals)
        lsqmat = np.array(lsqmat)

        step = np.linalg.lstsq(lsqmat, -residuals, rcond=None)[0]
        position += step

        if np.linalg.norm(step) < tolerance:
            break
   '''removing offset, the offset is used to avoid division by 0 in linear
regression'''
    position[0] = position[0]-500
    position[1] = position[1]-500


    position = np.trunc(position)

    return position



if __name__ == "__main__":

   '''this section is setting up the button and led indicator for testing
purposes'''
    chip = gpiod.Chip("gpiochip4")
    led = chip.get_line(led_pin)
    button = chip.get_line(button_pin)
    led.request(consumer="LED",type=gpiod.LINE_REQ_DIR_OUT)
    button.request(consumer="Button",type=gpiod.LINE_REQ_DIR_IN)

    '''open("/home/pi/Tracking_wifi/data.txt", "w").close() # delete the
content of the file and close the file
     open("/home/pi/Tracking_wifi/DATA1.txt", "w").close() # delete the
content of the file
     open("/home/pi/Tracking_wifi/DATA2.txt", "w").close() # delete the
content of the file
     open("/home/pi/Tracking_wifi/DATA3.txt", "w").close() # delete the
content of the file
     open("/home/pi/Tracking_wifi/DATA4.txt", "w").close() # delete the
content of the file
     open("/home/pi/Tracking_wifi/DATA5.txt", "w").close() # delete the
content of the file
     open("/home/pi/Tracking_wifi/DATA6.txt", "w").close() # delete the
content of the file
open first time to clear the files'''

    count = 0
  """ the testing phase is composed of moving the target device
    between 6 differnt positions, at each position the button is pressed,
    and the data of that position is saved to the corresponding file. A
    LED indicator is turned on during the computation"""

    while True:
        bstatus = button.get_value()
```

```
if bstatus:
    count = count + 1
    #scan and obtain network information in the area
    cells = scan_all_networks()
    Node_cell = append_cells(cells)
    Pos = position_estimate(Node_cell)
    tab = "\n"


    match count:
        case 1:

            data = open("/home/pi/Tracking_wifi/DATA1.txt", "a")
            data.write(str(Pos))
            data.write(tab)
            data.close()
        case 2:

            data = open("/home/pi/Tracking_wifi/DATA2.txt", "a")
            data.write(str(Pos))
            data.write(tab)
            data.close()
        case 3:

            data = open("/home/pi/Tracking_wifi/DATA3.txt", "a")
            data.write(str(Pos))
            data.write(tab)
            data.close()
        case 4:

            data = open("/home/pi/Tracking_wifi/DATA4.txt", "a")
            data.write(str(Pos))
            data.write(tab)
            data.close()
        case 5:

            data = open("/home/pi/Tracking_wifi/DATA5.txt", "a")
            data.write(str(Pos))
            data.write(tab)
            data.close()
        case 6:

            data = open("/home/pi/Tracking_wifi/DATA6.txt", "a")
            data.write(str(Pos))
            data.write(tab)
            data.close()

    if count == 6:
         count = 0
         print("done")
    led.set_value(1)
    time.sleep(10)

if bstatus==0:
      led.set_value(0)
```

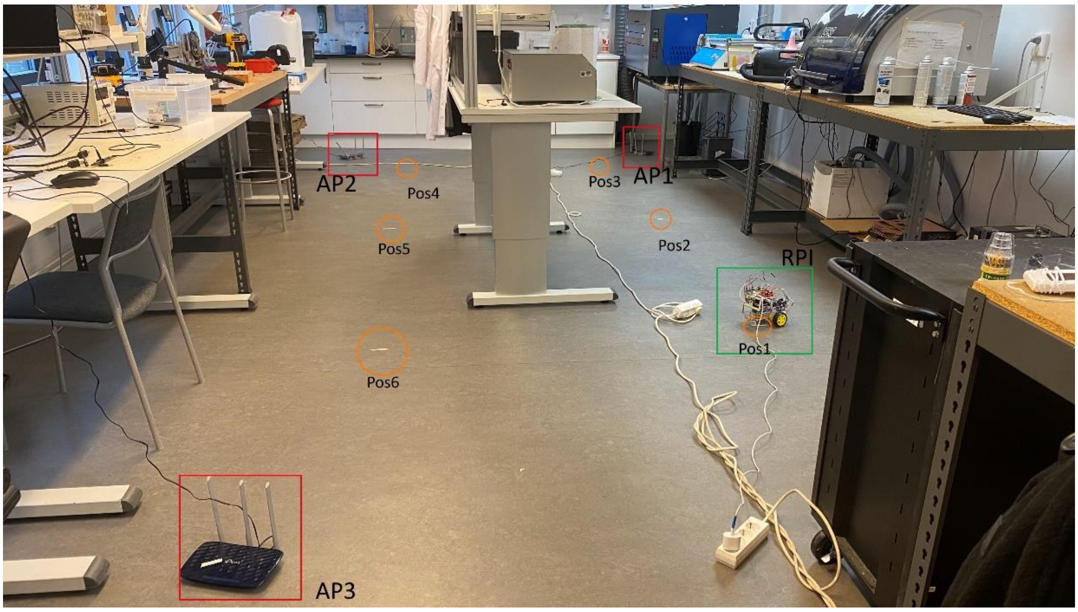

Appendix 2: The place where the test was conducted. Marked in red are the Aps, orange are the reference positions, and green is the receiver.

Appendix 3: a table containing the raw estimated position data with the Wi-Fi method.

walk	Position 1		position 2		position 3		position 4		position 5		position 6	
	X	Y	X	Y	X	Y	X	Y	X	Y	X	Y
Actual position	50	450	50	250	50	50	250	50	250	250	250	450
1	99	383	116	258	39	220	251	-228	12	461	167	466
2	20	490	114	206	-6	235	478	175	86	375	492	496
3	90	413	55	267	78	204	378	154	165	261	188	392
4	81	623	156	206	52	232	456	0	434	132	240	368
5	-213	354	197	139	170	199	407	126	-87	268	75	395
6	193	288	-68	148	71	-172	268	286	-8	360	97	678
7	69	802	124	162	104	99	416	43	417	291	187	422
8	-342	436	99	215	3	81	426	162	18	362	456	414
9	-87	485	156	201	113	153	388	168	290	-290	223	440
10	110	397	60	175	33	116	418	186	63	329	297	382
11	190	322	66	206	67	140	298	-119	65	295	431	417
12	-93	366	147	208	-10	215	564	298	263	248	115	391
13	-194	486	116	176	167	196	416	43	148	254	210	348
14	97	424	141	197	89	152	440	152	-182	242	18	579
15	-70	427	147	187	108	148	490	11	-30	351	278	446
16	92	602	-4	162	105	198	266	174	142	-232	175	412
17	-8	312	15	179	106	137	308	-266	18	275	15	534
18	-157	369	34	208	-83	145	359	118	486	258	3	501
19	-184	391	-151	176	43	198	410	-11	-50	393	273	357
20	-8	369	103	282	-7	185	134	-65	164	-131	458	485
21	85	304	-9	285	45	138	373	77	690	46	155	412
22	690	501	78	204	-1	124	160	-195	-14	303	123	403
23	-190	492	141	143	19	176	253	-182	-22	484	33	404
24	533	577	15	179	-64	139	268	122	20	708	97	373
25	-35	340	112	199	97	209	200	-120	-117	465	173	452
26	538	380	46	297	-171	85	210	-77	17	347	136	388

Appendix 4: Wiring diagram for RPP & RFM69HCW

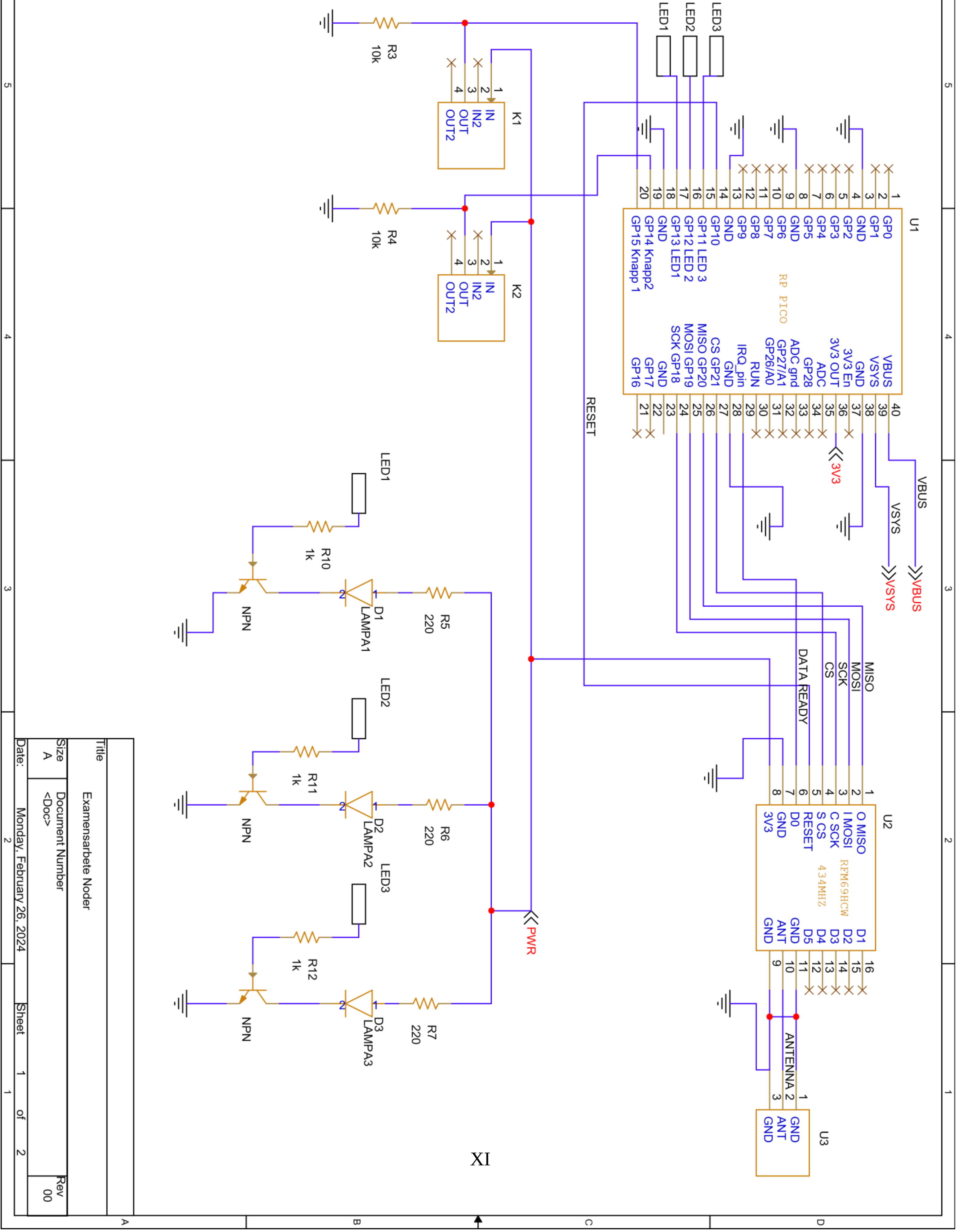

Appendix 5: Wiring diagram for power selector